

Ultra-low-frequency gravitational waves from individual supermassive black hole binaries as standard sirens

Ling-Feng Wang¹, Yue Shao¹, Jing-Fei Zhang¹, Xin Zhang^{1,2,3}

¹*Key Laboratory of Cosmology and Astrophysics (Liaoning) & College of Sciences, Northeastern University, Shenyang 110819, China*

²*National Frontiers Science Center for Industrial Intelligence and Systems Optimization, Northeastern University, Shenyang 110819, China*

³*Key Laboratory of Data Analytics and Optimization for Smart Industry (Ministry of Education), Northeastern University, Shenyang 110819, China*

Ultra-low-frequency gravitational waves (GWs) generated by individual inspiraling supermassive black hole binaries (SMBHBs) in the centers of galaxies may be detected by pulsar timing arrays (PTAs) in the future. These GW signals encoding absolute cosmic distances can serve as bright and dark sirens, having potential to be developed into a precise cosmological probe. Here we show that an SKA-era PTA consisting of 100 millisecond pulsars may observe about 25 bright sirens and 41 dark sirens during a 10-year observation. The bright sirens, together with the CMB data, have comparable capabilities to current mainstream data for measuring the equation of state of dark energy. The dark sirens could make the measurement precision of the Hubble constant close to that of current distance-ladder observation. Our results indicate that ultra-low-frequency GWs from individual SMBHBs are of great significance in exploring the nature of dark energy and measuring the Hubble constant.

Gravitational waves (GWs) are ripples in the fabric of spacetime, produced when large masses accelerate. The detection of GW150914¹, the first GW event of binary black hole coalescence, has marked the beginning of the era of GW astronomy. The luminosity distances of GW sources, encoded in the amplitudes of GW waveforms, can be inferred from GW measurements, usually referred to as “standard sirens”². The standard sirens with electromagnetic (EM) counterparts can be used as “bright sirens” to directly constrain cosmological parameters via the distance-redshift relation²⁻⁴. For the standard sirens without EM counterparts, one can use GW signals to find their potential host galaxies in galaxy catalogs. A statistical analysis of these galaxies’ redshifts together with the GW signals can also provide constraints on cosmological parameters and such GW data are usually called “dark sirens”^{2,5,6}.

Typical sources of standard sirens are compact binary coalescences, including stellar-mass compact binaries and supermassive black hole binaries (SMBHBs). Stellar-mass compact binaries, such as binary neutron stars (BNSs) and stellar-mass binary black holes (SBBHs), can be detected by ground-based GW detectors in the frequency band between $\mathcal{O}(10) - \mathcal{O}(10^3)$ Hz. BNS coalescences are expected to have EM counterparts and have been experimentally confirmed by the GW170817 event⁷ that is the only available bright siren till now, providing a $\sim 14\%$ measurement for the Hubble constant H_0 . SBBH coalescences are commonly thought to have no EM counterparts but they can serve as dark sirens. 47 such GW sources from the Third LIGO-Virgo-KAGRA Gravitational-Wave Transient Catalog provide a $\sim 19\%$ measurement of the Hubble constant with the dark siren method⁸. In the future, the third-generation ground-based GW detectors (the Einstein Telescope⁹ and the Cosmic Explorer¹⁰) enable ones to acquire numerous available standard

sirens of stellar-mass compact binaries¹¹.

Low-frequency GWs emitted by SMBHBs with masses of $10^4 - 10^8 M_{\odot}$ can be detected in the mHz frequency band by the planned space-borne GW observatories, e.g., the Laser Interferometer Space Antenna¹², Taiji¹³, and TianQin¹⁴. These SMBHBs may produce EM emissions due to their surrounding gas-rich environments and external magnetic fields^{15,16}, and therefore they are also expected to serve as bright sirens¹⁷⁻²¹. Recent studies show that such SMBHBs can also serve as dark sirens and provide precise measurements for H_0 ^{22,23}.

Ultra-low-frequency GWs emitted by SMBHBs with masses of $10^8 - 10^{10} M_{\odot}$ are expected to be detected in the nHz frequency band by the natural galactic-scale detector comprised of an array of millisecond pulsars (MSPs), usually referred to as “pulsar timing array” (PTA). When GWs pass between pulsars and the Earth, the paths of the pulsar signals change, thus affecting the times of arrival (ToAs) of radio pulses. Nanohertz GWs from individual inspiraling SMBHBs could be detected by monitoring the spatially correlated fluctuations of ToAs induced by GWs. With the concept proposed decades ago, there are three major PTA projects, namely, the Parkes Pulsar Timing Array²⁴, the European Pulsar Timing Array²⁵, and the North American Nanohertz Observatory for Gravitational Waves²⁶. They have also been combined to form the International Pulsar Timing Array²⁷ aimed at significantly enhancing sensitivities. So far, most of the efforts have been devoted to detecting the stochastic gravitational wave background (SGWB)²⁸⁻³⁰. Although challenging, the detections of individual SMBHBs will have immense scientific return. The capability of detecting individual SMBHBs using PTAs has been investigated in Refs.³¹⁻³³. With the participation of more

advanced radio telescopes such as the Five-hundred-meter Aperture Spherical Telescope (FAST)³⁴ in China and the planned Square Kilometre Array (SKA)³⁵, there is a great possibility that GWs produced by individual SMBHBs (other than SGWBs) could be detected by SKA-era PTAs³⁶.

Recently, it was proposed in Ref.³⁷ that inspiraling SMBHBs to be detected by PTAs may also be used as bright sirens. The luminosity distances of currently available SMBHB candidates detected by EM observations³⁸ with known redshifts may be measured by the PTA GW observations, then the distance-redshift relation can be used to constrain cosmological parameters. In Ref.³⁷, a preliminary study on constraining dark energy parameters was performed, in which only the equation-of-state (EoS) parameters of dark energy are set free but other cosmological parameters are all fixed. Obviously, such a treatment cannot reveal how well the PTA nanohertz GW observations could constrain cosmological parameters. Actually, the most prominent advantage of GW bright sirens in cosmological parameter estimations is that they can break the degeneracies between cosmological parameters^{21,39–41}. The capabilities of the bright sirens from ground-based detectors and space-borne observatories of breaking the parameter degeneracies have been widely discussed (see Ref.⁴² for a recent review), but the relevant studies on the standard sirens from PTA observations are still absent. Here the first question to be answered is what role the ultra-low-frequency GW bright sirens can play in breaking the degeneracies between cosmological parameters.

Although the SMBHB bright sirens from the PTA observations are thought to be useful in measuring cosmological parameters, they also have limitations, because the SMBHB candidates

with known redshifts may not really be SMBHBs and the actual detected SMBHBs may not be the members of these candidates. Therefore, it is important to find a way to measure cosmological parameters when the SMBHB bright sirens are not available. We propose that SMBHBs detected by PTAs may serve as dark sirens. Dark sirens require suitable galaxy catalogs to provide potential host galaxies of SMBHBs. Since the redshifts of the existing galaxy catalogs are relatively low, only SMBHBs in the local Universe might be used as dark sirens. Along this line, the second question we wish to answer is whether SMBHBs in the local Universe can be used as ultra-low-frequency GW dark sirens to precisely measure cosmological parameters.

In this work, we analyze the ability of SKA-era PTAs to detect the existing SMBHB candidates and the local-Universe SMBHBs by simulating the timing residuals of pulsar signals, and then use the mock GW bright-siren and dark-siren data to perform cosmological parameter estimations. The system of units in which $G = c = 1$ is adopted in this paper.

Results

The number of available MSPs, N_p , in the SKA-era PTAs is still uncertain⁴³, and therefore we select 100, 200, and 500 MSPs within 3 kpc from the Earth, obtained from the Australia Telescope National Facility (ATNF) pulsar catalog⁴⁴, to construct PTAs. The root mean square (rms) of timing residual, σ_t , reflecting the stability of the pulsar and the quality of the ToA data, consists of red noise and white noise. Since the GW strain induced by an individual source in the frequency domain appears as a single peak on the PTA-detection time scale, which is essentially different

from frequency-dependent SGWB³², the red noise mainly affects the detection of SGWB while it is less critical on the detections of individual sources, especially at relatively high frequency. For simplicity, we ignore the influence of the red noise in this work. The white noise mainly includes jitter noise and radiometer noise. The jitter noise will dominate for most bright pulsars and the total white noises are around $10 \sim 50$ ns⁴⁵. Considering that FAST and SKA could make the noise lower, we expect that σ_t could reach ~ 20 ns for SKA-era PTAs. We consider two cases of $\sigma_t = 20$ ns and $\sigma_t = 100$ ns for comparison. Here we assume that the GW spectrum induced by SGWB can be well measured in the forthcoming years and the GW signals from individual SMBHBs can be resolved from SGWB⁴⁶, therefore we do not consider SGWB in this work. We assume that the ToA data are obtained via monitoring the pulses from MSPs with the typical cadence of two weeks and the observation span is 10 years³⁷.

We analyze the ability of SKA-era PTAs to detect SMBHBs by simulating the timing residuals (see Methods). The detection curves of SKA-era PTAs, averaged over the sky locations of the GW sources, are plotted in Fig. 1 by using the `hasasia` package^{47,48}. The solid dots without black borders represent 154 SMBHB candidates and the solid dots with black borders represent 84 SMBHBs simulated from the 2 Micron All Sky Survey (2MASS)⁴⁹ Extended Source Catalog⁵⁰. As N_p increases and σ_t decreases, the more sensitive detection curves enable ones to detect more SMBHBs. The dotted curves ($\sigma_t = 20$ ns) are obviously lower than the solid curves ($\sigma_t = 100$ ns), indicating that the rms timing residual has a more dominating effect than the number of MSPs on the detections of SMBHBs.

To simulate GW bright-siren data, we adopt 154 currently available SMBHB candidates^{38,51–57}, mainly obtained via the observations of periodic variations in their light curves^{38,52,53} from the Catalina Real-time Transient Survey and the Palomar Transient Factory⁵⁸. These methods are appropriate for SMBHBs in the inspiral phase. Actually, SMBHBs in the merger phase are likely to emit dual jets⁵⁹ that may be detected by future telescopes, such as the Vera C. Rubin Observatory (formerly known as LSST)⁶⁰ and the European Extremely Large Telescope⁶¹. These EM signals can also be used as EM counterparts to provide redshifts⁶². According to the analysis in Refs.^{21,62}, in a 5-year observation, dozens of SMBHBs ($10^4 - 10^8 M_\odot$) with the dual-jet EM counterparts could be observed by space-borne observatories in the mHz band. Usually, SMBHBs in the PTA band will inspiral for a long time and we need to wait hundreds of years for the merger phase. Therefore, it is more difficult to detect the merger-phase EM signals for PTA-band SMBHBs.

The relative errors of the luminosity distances ($\Delta d_L/d_L$) of the mock SMBHB bright and dark sirens as a function of signal-to-noise ratio (SNR), ρ , are shown in Fig. 2. The corresponding numbers of detected bright and dark sirens ($\rho > 10$) are shown in Table 1. In the case of $N_p = 100$, the number of detected bright sirens increases from 14 ($\sigma_t = 100$ ns) to 25 ($\sigma_t = 20$ ns) and the number of detected dark sirens increases from 13 ($\sigma_t = 100$ ns) to 41 ($\sigma_t = 20$ ns). Although the number of MSPs can also affect the detection number of SMBHBs, its effect is not as obvious as σ_t . For example, in the case of $\sigma_t = 100$ ns, the number of detected bright sirens increases from 14 ($N_p = 100$) to 15 ($N_p = 500$) and the number of detected dark sirens increases from 13 ($N_p = 100$) to 27 ($N_p = 500$). This indicates that the rms timing residual is the most important factor in reducing the errors of luminosity distances. Our results show that about 100 MSPs are

sufficient for detecting individual SMBHBs, if the timing measurement could reach high-enough precision.

Assuming different N_p and σ_t , we simulate six sets of bright-siren data that contain d_L , Δd_L , and the redshift z of the SMBHB candidates (see Methods). We use these bright-siren data to constrain the Λ CDM and w CDM models, respectively. The constraint results of the Λ CDM model solely from the bright-siren data are listed in Table 1. We define the constraint precision of the parameter ξ as $\varepsilon(\xi) = \sigma(\xi)/\xi$ with $\sigma(\xi)$ representing the marginalized absolute error. In the case of $\sigma_t = 100$ ns, as N_p increases from 100 to 500, $\varepsilon(H_0)$ decreases from 2.1% to 1.8%. In the case of $N_p = 100$, as σ_t decreases from 100 ns to 20 ns, $\varepsilon(H_0)$ decreases from 2.1% to 1.5%. We note that reducing σ_t is more effective than increasing N_p on improving the constraining capability of bright sirens. If σ_t could reach 20 ns, 100 MSPs are sufficient to make the measurement precision of H_0 comparable to that of the current cosmic distance-ladder observation.

In the w CDM model, the cosmic microwave background (CMB) data cannot provide tight constraints on the EoS parameter of dark energy (w), because CMB encodes the information of the early Universe, while dark energy becomes dominant in the late Universe. Nevertheless, Fig. 3 shows that the CMB data and the bright-siren data (simply referred to as the PTA data) have distinct degeneracy orientations in the w - H_0 plane, indicating that although the PTA data alone cannot constrain w well either, it can provide tight constraints on H_0 , thus breaking the degeneracy between the parameters w and H_0 . Extended Data Table 1 shows that, in the case of $N_p = 100$ and $\sigma_t = 20$ ns, the combination of the CMB and PTA data gives the relative error $\varepsilon(w) = 4.7\%$, which

is roughly comparable with the result of *Planck* 2018 TT,TE,EE+lowE+lensing+SNe+BAO⁶³. The results suggest that the SMBHB bright sirens will be a useful probe to explore the nature of dark energy.

To simulate GW dark-siren data, we consider 5119 galaxies in the 2MASS catalog as SMBHBs' possible host galaxies. We simulate 84 SMBHBs according to the probability of a galaxy hosting an SMBHB in the PTA band (see Methods). Furthermore, we simulate the GW signals emitted by the 84 SMBHBs and consider those with $\rho > 10$ as detected SMBHBs. Table 1 shows the numbers of detected SMBHBs in different cases. For these SMBHBs, we determine their localization volumes by the Fisher matrix (see Methods). The redshifts of the galaxies within the localization volumes can be utilized to infer the posterior distribution of cosmological parameters. Since the dark sirens are simulated in the local Universe in which the d_L - z relation is weakly dependent on cosmological models, these data cannot constrain w well. Therefore, we only calculate the posterior distribution of H_0 via the Bayesian analysis method (see Methods).

The results of the SMBHB dark sirens are shown in Fig. 4 and Table 1. In the case of $\sigma_t = 100$ ns, increasing N_p from 100 to 500 can significantly improve the measurement of H_0 . The 1σ errors of H_0 with $\sigma_t = 20$ ns are obviously smaller than those with $\sigma_t = 100$ ns. It is worth noting that even with only 100 MSPs ($N_p = 100$ and $\sigma_t = 20$ ns), the precision of H_0 could reach $\sim 1.8\%$. Compared with the SMBHB bright sirens, the SMBHB dark sirens have a similar ability in measuring H_0 . This indicates that even if it is difficult to detect EM counterparts of SMBHBs in the future, dark sirens could solely provide precise measurement of H_0 . The bright and dark sirens

have potential to complement each other to provide precise measurements for both w and H_0 .

Discussion

In this work, we assume that the cadence of monitoring the pulses from MSPs is two weeks³⁷ and consider $N_p = 100, 200, 500$ respectively. Actually, observing 500 MSPs is not achievable with this cadence due to the time required for each observation, and therefore the case of $N_p = 500$ is just used as an extreme case for comparison. To show the effect of the cadence, we consider another case with the cadence of one month instead of two weeks. In this case, 23 bright sirens could be observed during 10 years when $N_p = 100$ and $\sigma_t = 20$ ns, and the measurement precision of H_0 reach 1.66%, similar with the result obtained with the cadence of two weeks [$\varepsilon(H_0) = 1.47\%$], indicating that even if the observation time is reduced by a factor of 2, SMBHB standard-siren data could still maintain tight constraints on H_0 .

In the analysis of dark sirens, all SMBHBs are simulated at $z < 0.05$ based on the 2MASS catalog. In the future, the Stage IV space-based telescopes, such as the China Space Station Telescope (CSST)⁶⁴, the Vera C. Rubin Observatory, and the Euclid space mission⁶⁵, could provide galaxy catalogs at higher redshift. According to our preliminary estimation, CSST is expected to provide a complete galaxy catalog up to $z \sim 0.3$ at which $\mathcal{O}(10^3) - \mathcal{O}(10^4)$ SMBHBs could be observed by PTAs. Although the measurements on H_0 are mainly contributed by the local-Universe SMBHBs considered in this work, larger numbers of SMBHB dark sirens may help to measure other cosmological parameters, such as the EoS parameter of dark energy.

The chirp mass, M_c , depends on the mass ratio between the two black holes forming an SMBHB. Therefore, the mass ratio affects not only SNRs of GWs but also the probability of the existence of an SMBHB in a galaxy⁶⁶. This two effects both affect the constraint precision of cosmological parameters. We define $q = m_1/m_2$ as the mass ratio with $q \in (0, 1]$. The results in the main text is based on the assumption that q is randomly chosen between $[0.25, 1]$ with a log-normal distribution⁶⁷. We discuss the effect of q in detail in Methods and show the constraint results of H_0 with different q values in Extended Data Table 2.

Compared with the GW standard sirens in other frequency bands, the ultra-low-frequency GW standard sirens have some advantages. (i) The masses of the GW sources are at the top of the mass range of SMBHBs, leading to higher SNRs. Fig. 2 shows that the highest SNR could reach ~ 700 . Such high SNRs are helpful to accurately localize GW sources and thus contribute to the precise measurements of H_0 . (ii) Unlike BNSs that are thought to emit EM signals only in the merger phase, SMBHBs could produce observable EM signals in the inspiral phase, i.e., the characteristic signals of the SMBHB candidates. The inspiral-phase EM signals not only provide redshifts for bright sirens but also provide the early alerts for GW detections, which can help us to choose MSPs at suitable sky positions to obtain the best sensitivity in the direction of the GW source. (iii) When an SMBHB evolves to the late stage, the GW frequency may fall in the frequency band of space-borne GW detectors. Although most PTA-band SMBHBs inspiral for a long time, in a few cases, for example, an SMBHB with $M \sim 10^9 M_\odot$, $z \lesssim 1$, and $f_0 \sim 10^{-7}$ is expected to enter the merger phase after 17 years. Once such cases are discovered, the joint observation in the mHz and nHz frequency bands can be realized, which is helpful to localize GW

sources and explore the various physical properties of SMBHBs.

We conclude that ultra-low-frequency GWs emitted by individual SMBHBs can serve as both bright and dark sirens and have promising potential in two aspects. (i) The bright-siren data could effectively break the cosmological-parameter degeneracy inherent in the CMB data. The bright-siren data combined with the CMB data have a comparable capability to the mainstream observational data (*Planck* 2018 TT,TE,EE+lowE+lensing+SNe+BAO) for measuring w . (ii) The dark sirens in the local Universe have high SNRs and could be well localized, making the measurement precision of H_0 close to that of the current distance-ladder observation. The bright and dark sirens can complement each other to measure both w and H_0 precisely. Ultra-low-frequency GWs detected by SKA-era PTAs could be developed into a precise late-Universe probe to explore the nature of dark energy and measure the Hubble constant.

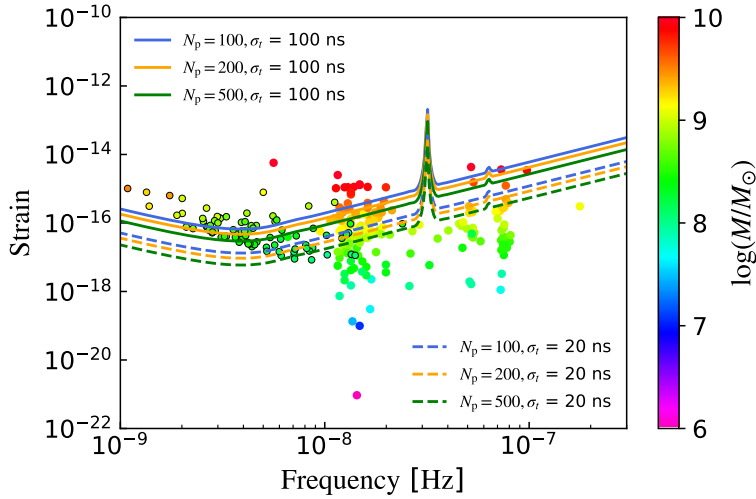


Figure 1 | Detection curves of SKA-era PTAs with a 10-year observation time span.

The solid and dotted lines represent the cases of $\sigma_t = 100$ ns and $\sigma_t = 20$ ns, respectively.

The data points represent the GW strain amplitudes (h_0) when $f = f_0$, with $h_0 = 2[M_c(1 + z)]^{5/3}(\pi f)^{2/3}d_L^{-1.37}$ and f_0 the GW frequency at the time of the first observation. The solid dots without black borders represent 154 SMBHB candidates and the solid dots with black borders represent 84 SMBHBs simulated from the 2MASS catalog.

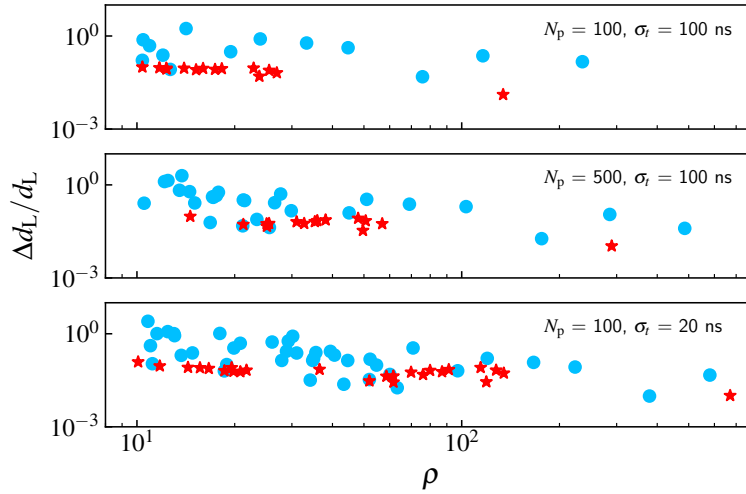


Figure 2 | Measurement precision of luminosity distance ($\Delta d_L/d_L$) as a function of SNR (ρ). The red stars and the blue dots represent the detected SMBHBs with $\rho > 10$, used as the bright and dark sirens, respectively. The impacts of N_p and σ_t on the SMBHB detections can be explicitly seen.

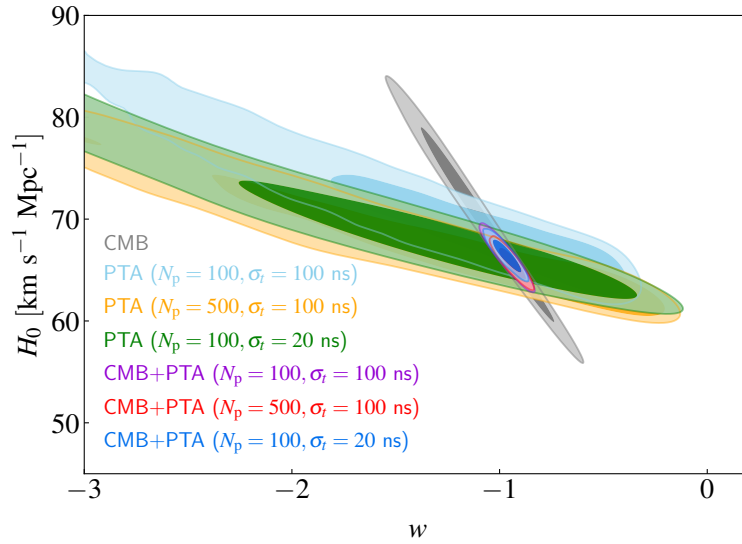


Figure 3 | 2D marginalized contours (68.3% and 95.4% confidence level) in the w - H_0 plane for the w CDM model by using the CMB, PTA, and CMB+PTA data. Here the PTA data refer to the mock GW bright-siren data.

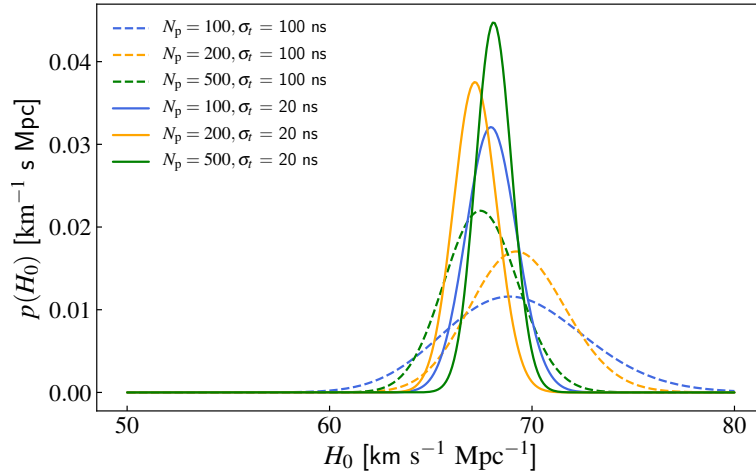


Figure 4 | 1D posterior distribution of H_0 inferred from the mock GW dark-siren data. The dotted and solid lines represent the cases of $\sigma_t = 100$ ns and $\sigma_t = 20$ ns, respectively. The errors of H_0 become smaller as N_p increases and σ_t decreases.

N_p	$\sigma_t(\text{ns})$	bright siren			dark siren		
		N_s	$\sigma(H_0)$	$\varepsilon(H_0)$	N_s	$\sigma(H_0)$	$\varepsilon(H_0)$
100	100	14	1.4	0.0209	13	3.458	0.0500
200	100	14	1.3	0.0193	19	2.350	0.0339
500	100	15	1.2	0.0183	27	1.824	0.0270
100	20	25	1.0	0.0147	41	1.248	0.0184
200	20	40	1.0	0.0151	49	1.066	0.0159
500	20	53	0.95	0.0141	56	0.895	0.0131

Table 1 | Relative errors of H_0 in the ΛCDM model. The GW bright-siren data are simulated based on the 154 SMBHB candidates and the GW dark-siren data are simulated based on the 5119 galaxies in the 2MASS catalog. N_s is the number of detected SMBHBs ($\rho > 10$) and $\varepsilon(H_0)$ is the relative error of H_0 .

Methods

The detection of individual SMBHBs. GW signals are detected in the timing residuals of MSPs by removing model-predicted ToAs from the observational ToA data. The timing residuals induced by a single GW source, measured at time t on the Earth, can be written as

$$s(t, \hat{\Omega}_s, \hat{\Omega}_p) = F_+(\hat{\Omega}_s, \hat{\Omega}_p)\Delta A_+(t) + F_\times(\hat{\Omega}_s, \hat{\Omega}_p)\Delta A_\times(t), \quad (1)$$

with $F_{+,\times}(\hat{\Omega}_s, \hat{\Omega}_p)$ the geometric factors, equivalent to the antenna pattern functions of laser interferometric GW detections³⁷. $\hat{\Omega}_s$ and $\hat{\Omega}_p$ are the unit vectors pointing from the GW source and the pulsar to the observer, respectively, determined by the sky positions of the GW source (α_s, β_s) and the pulsar (α_p, β_p) . Extended Data Fig. 1 shows the sky positions of the selected 500 MSPs used in this work. $\Delta A_{+,\times}(t) = A_{+,\times}(t) - A_{+,\times}(t_p)$ is the difference between the Earth term $A_{+,\times}(t)$ and the pulsar term $A_{+,\times}(t_p)$, with t_p the time at which GW passes the MSP⁶⁸.

$\Delta A_{+,\times}(t)$ encodes the GW strain amplitude $h(t)$. We assume that SMBHBs inspiral in circular orbits, and then $h(t)$ can be written as

$$h(t) = 2 \frac{(G\mathcal{M}_c)^{5/3}}{c^4} \frac{[\pi f(t)]^{2/3}}{d_L}. \quad (2)$$

Here, $\mathcal{M}_c = M_c(1+z)$ represents the redshifted chirp mass and M_c is the chirp mass defined as $M_c = \eta^{3/5}M$. $M = m_1 + m_2$ is the total mass of the binary system with component masses m_1 and m_2 , and $\eta = m_1m_2/(m_1 + m_2)^2$ is the symmetric mass ratio. d_L represents the luminosity distance of the GW source. The GW frequency $f(t)$ is given by

$$f(t) = \left[f_0^{-8/3} - \frac{256}{5} \pi^{8/3} \left(\frac{G\mathcal{M}_c}{c^3} \right)^{5/3} t \right]^{-3/8}, \quad (3)$$

where $f_0 = 2f_{\text{orb}}$ is the GW frequency at the time of the first observation. Here $f_{\text{orb}} = (2\pi T)^{-1}$ is the orbit frequency and T is the orbital periods of SMBHBs. When simulating the GW signals of bright sirens, we calculate f_0 using the orbital periods of the 154 SMBHB candidates^{38,51–57}. When simulating the GW signals of dark sirens, we calculate f_0 using Eq. (11).

The SNR (ρ) of the GW signal detected by a PTA is given by

$$\rho^2 = \sum_{i=1}^{N_p} \sum_{n=1}^N \left[\frac{s_i(t_n)}{\sigma_{t,i}} \right]^2, \quad (4)$$

where N is the total number of data points for each MSP, N_p is the number of MSPs, $s_i(t_n)$ is the timing residual induced by the GW signal in the i -th MSP at time t_n [see Eq. (1)], and $\sigma_{t,i}$ is the rms of the timing residual of the i -th MSP.

Fisher information matrix is adopted to estimate the parameters of GW sources. For a PTA including N_p independent MSPs, the Fisher matrix \mathbf{F} is expressed as

$$F_{ab} = \sum_{i=1}^{N_p} \sum_{n=1}^N \frac{\partial s_i(t_n)}{\sigma_{t,i} \partial \theta_a} \frac{\partial s_i(t_n)}{\sigma_{t,i} \partial \theta_b}, \quad (5)$$

where $\boldsymbol{\theta}$ denotes the free parameters to be estimated. The instrumental error of the parameter θ_a is estimated as $\Delta\theta_a = \sqrt{(F^{-1})_{aa}}$. Here, nine parameters are taken into account in the Fisher matrix, including eight parameters of a GW source and the pulsar distance, i.e., M_c , α_s , β_s , ι , ψ , ϕ_0 , f_0 , d_L , and d_p . The inclination angle ι is randomly chosen between $[0, \pi]$. The polarization angle ψ and the initial phase ϕ_0 of SMBHBs are randomly chosen between $[0, 2\pi]$.

In addition to the instrumental error (Δd_L^{inst}) estimated by the Fisher matrix, the total error of

d_L should also include the weak lensing error (Δd_L^{lens})⁶⁹ and the peculiar velocity error (Δd_L^{pv})⁷⁰,

$$\Delta d_L = \sqrt{(\Delta d_L^{\text{inst}})^2 + (\Delta d_L^{\text{lens}})^2 + (\Delta d_L^{\text{pv}})^2}, \quad (6)$$

with

$$\Delta d_L^{\text{lens}}(z) = d_L(z) \times 0.066 \left(\frac{1 - (1+z)^{-0.25}}{0.25} \right)^{1.8}, \quad (7)$$

$$\Delta d_L^{\text{pv}}(z) = d_L(z) \times \left[1 + \frac{c(1+z)^2}{H(z)d_L(z)} \right] \frac{\sqrt{\langle v^2 \rangle}}{c}, \quad (8)$$

where $H(z)$ is the Hubble parameter and $\sqrt{\langle v^2 \rangle}$ is the peculiar velocity of the GW source with $\sqrt{\langle v^2 \rangle} = 500 \text{ km s}^{-1}$ ⁷¹. Since Δd_L^{lens} is relatively small at $z < 0.1$ ⁷², we consider this error only when simulating the bright-siren data and ignore it when simulating the dark-siren data. When simulating the bright-siren data, we use Eq. (8) to calculate the peculiar velocity error of d_L and add it to the total error of d_L ; when simulating the dark-siren data, we consider the peculiar-velocity effect in the error of z instead of in the error of d_L [see Eq. (15)].

SMBHB bright sirens. When we simulate the GW bright-siren data, we adopt 154 currently available SMBHB candidates obtained from various characteristic signatures. The redshifts of these SMBHB candidates are taken from Refs.^{38,51–57}. Extended Data Fig. 2 shows these SMBHB candidates in the z - M plane. We use their redshifts to calculate their luminosity distances based on the Λ CDM model in which the cosmological parameters are set to the *Planck* 2018 results.

We use Eqs. (1)–(3) to simulate the GW signals emitted by these SMBHB candidates. Fig. 1 shows the strain amplitudes (when $f = f_0$) of the GW signals. Here we only plot the strain amplitudes when $f = f_0$, because a simple calculation using Eq. (3) shows that the variation of

the GW frequency of an inspiraling SMBHB with $M = 10^9 M_\odot$ and $f_0 = 10^{-7}$ Hz in a 10-year observational time span is 4.36×10^{-9} Hz, and this variation is so minuscule that the amplitude of the GW strain undergoes only negligible changes over the given time span.

We use Eq. (4) to calculate SNRs of the SMBHB candidates. We use N_s to represent the number of SMBHBs with $\rho > 10$, shown in Table 1. For these SMBHBs, we use the Fisher matrix to estimate the errors of luminosity distances. d_L , Δd_L , and z compose the bright-siren data and can be used to constrain cosmological parameters via the d_L - z relation. Two representative sets of the GW bright-siren data are shown in Extended Data Fig. 3. The numbers of detected bright sirens in the case of $\sigma_t = 20$ ns are much larger than those in the case of $\sigma_t = 100$ ns for the same number of MSPs. Improved SNRs of the GW events by decreasing σ_t reduce the measurement errors of luminosity distances.

Here we consider the base Λ CDM model ($w = -1$) and the w CDM model ($w = \text{constant}$).

The d_L - z relation can be written as

$$d_L = \frac{(1+z)}{H_0} \int_0^z \frac{dz'}{\sqrt{\Omega_m(1+z')^3 + (1-\Omega_m)(1+z')^{3(1+w)}}, \quad (9)$$

where Ω_m represents the current matter density parameter. The constraint results of the base Λ CDM model are shown in Extended Data Fig. 4 and listed in Table 1. The constraint results of the w CDM model are shown in Fig. 3 and listed in Extended Data Table 1.

Smaller q could decrease the chirp mass of SMBHBs and thus decrease SNRs. According to our calculation, two SMBHBs ($z = 0.05$ and $M = 10^9 M_\odot$) with $q = 1$ and $q = 0.1$ have SNR

= 19.52 and SNR = 6.45, respectively, when a PTA with $N_p = 100$ and $\sigma_t = 20$ ns is considered. We set the range of q to $[q_{\min}, 1]$ according to the log-normal distribution. The main results in this paper are based on $q_{\min} = 0.25$. To show the effect of q more explicitly, we show the constraint results of H_0 with different q_{\min} values in Extended Data Table 2. We consider four cases, i.e., $q_{\min} = 1, 0.25, 0.1$ and 0.01 , where $q_{\min} = 1$ indicates that q is fixed at 1. It is shown that, for the bright-siren data, the values of q_{\min} have negligible effects on constraining H_0 .

SMBHB dark sirens. For dark sirens, we consider 5119 galaxies in the 2MASS catalog as SMBHBs' possible host galaxies. These galaxies are in the local Universe ($z < 0.05$) and the 2MASS catalog can be considered complete in this redshift range⁶⁷. The mass distribution of these galaxies is between 10^{11} – $10^{12} M_{\odot}$ ^{43,67}. We estimate the masses of SMBHBs in these galaxies according to the M - M_{buldge} relationship, with M_{buldge} the bulge mass of a galaxy⁷³.

The probability that a galaxy hosts an SMBHB in the PTA band, p_j , can be written as

$$p_j = \frac{t_{c,j}}{T_{\text{life}}} \int_{0.25}^1 d\mu_{\star} \frac{dN}{dt} (M_{\star}, \mu_{\star}, z') T_{\text{life}}. \quad (10)$$

Here $t_{c,j} = (5/256)(\pi f_{\text{low}})^{-8/3}(GM_c/c^3)^{-5/3}$ is the time to SMBHB coalescence in the j -th galaxy, with $f_{\text{low}} = 1$ nHz being the lower limit of the PTA band. T_{life} is the effective lifetime of an SMBHB^{67,74,75}. $dN/dt (M_{\star}, \mu_{\star}, z')$ is the galaxy merger rate from the Illustris cosmological simulation project^{76,77}, with M_{\star} the stellar masses of the galaxies, μ_{\star} the progenitor stellar mass ratio, and z' the redshift at which the galaxies merge. We obtain the number of SMBHBs in the galaxy catalog by $N_{\text{SMBHB}} = \sum_j p_j$ ^{76,77}. Eq. (10) shows that p_j depends on $t_{c,j}$, and $t_{c,j}$ is related to M_c that is determined by q . Therefore, q could affect the merger probability of SMBHBs and further

affect the number of mock SMBHBs. As shown in Extent Data Table 2, smaller values of q_{\min} increase the numbers of both mock and detected SMBHBs. As q_{\min} decreases from 1 to 0.01, the number of mock SMBHBs increases from 54 to 197. The main results of this paper are based on the assumption of $q_{\min} = 0.25$. Under this assumption, we find that there are approximately 84 SMBHBs in the total 5119 galaxies. Then we randomly select 84 galaxies from the total galaxies as SMBHBs' host galaxies according to the probability distribution p_j .

Extended Data Fig. 5 shows the 84 SMBHBs in the z - M plane. Fig. 1 shows the strain amplitudes (when $f = f_0$) of the GW signals emitted by the 84 SMBHBs, with f_0 calculated by the following formula,

$$f_0 = \pi^{-1} \left(\frac{G\mathcal{M}_c}{c^3} \right)^{-5/8} \left(\frac{256}{5} t_c \right)^{-3/8}, \quad (11)$$

where t_c is taken from a uniform distribution in [100 yr, 26 Myr].

Using the GW signal, we can localize the GW source within a localization volume. Fig. 2 shows the relative errors of luminosity distances, $\Delta d_L/d_L$, as a function of SNR. By matching the localization volume to the galaxy catalog, we can find the host galaxy of the GW source. The localization volume usually contains more than one galaxy, and thus we need to consider these galaxies' redshifts in a statistical way. The Bayesian analysis is a statistical method commonly used for dark sirens.

In the Bayesian method, the posterior distribution of H_0 can be written as

$$p(H_0 | \mathcal{D}_{\text{GW}}, \mathcal{D}_{\text{EM}}) \propto p(\mathcal{D}_{\text{GW}}, \mathcal{D}_{\text{EM}} | H_0) p(H_0), \quad (12)$$

where \mathcal{D}_{GW} and \mathcal{D}_{EM} represent the GW and EM data, respectively. $p(H_0)$ represents the prior probability of H_0 , assumed to be uniformly distributed in the interval $[50, 80]$ $\text{km s}^{-1} \text{Mpc}^{-1}$. For a single GW event, the likelihood term, $p(\mathcal{D}_{\text{GW}}, \mathcal{D}_{\text{EM}}|H_0)$, can be written as

$$p(\mathcal{D}_{\text{GW}}, \mathcal{D}_{\text{EM}}|H_0) = \frac{\int p(\mathcal{D}_{\text{GW}}|d_L(z, H_0), \alpha, \beta)p(\mathcal{D}_{\text{EM}}|z, \alpha, \beta)p_0(z, \alpha, \beta)dzd\alpha d\beta}{\gamma(H_0)}. \quad (13)$$

$p(\mathcal{D}_{\text{GW}}|d_L(z, H_0), \alpha, \beta)$ in Eq. (13) is the likelihood of the GW data, expressed as

$$p(\mathcal{D}_{\text{GW}}|d_L(z, H_0), \alpha, \beta) \propto e^{-\chi^2/2}, \quad (14)$$

with $\chi^2 = (\mathbf{x} - \mathbf{x}_{\text{gw}})^T \mathbf{C}^{-1} (\mathbf{x} - \mathbf{x}_{\text{gw}})$. Here $\mathbf{x} = (d_L(z, H_0), \alpha, \beta)$ represents an arbitrary three-dimensional (3D) position in the sky. $\mathbf{x}_{\text{gw}} = (d_{L,s}, \alpha_s, \beta_s)$ represents the 3D position of the GW source, that is, the 3D position of the true host galaxy in our simulation. We calculate $d_{L,s}$ with the galaxies' redshifts (z_s) by assuming the Λ CDM model and setting the cosmological parameters to the *Planck* 2018 results. \mathbf{C} is the 3×3 covariance matrix only relevant to (d_L, α, β) , obtained from the Fisher matrix. We use $\chi^2 = 11.34$ (corresponding to 99% confidence) to determine the boundary of GW source's localization volume. If the position of a galaxy satisfies $\chi^2 < 11.34$, we consider this galaxy to be within the localization volume and regard it as a potential host galaxy of the GW source. We define N_{in} to describe the number of potential host galaxies. Generally, a small value of N_{in} means a strong ability to localize the GW source. Extended Data Fig. 6 shows the numbers of SMBHBs satisfying $N_{\text{in}} < 10$. It can be seen that more SMBHBs satisfy $N_{\text{in}} < 10$ as N_p increases and σ_t decreases. Here N_{in} is calculated by fixing $H_0 = 67.36 \text{ km s}^{-1} \text{Mpc}^{-1}$.

$p(\mathcal{D}_{\text{EM}}|z, \alpha, \beta)$ in Eq. (13) is the likelihood of the EM data and is given by

$$p(\mathcal{D}_{\text{EM}}|z, \alpha, \beta) = \frac{1}{N_{\text{in}}} \sum_{j=1}^{N_{\text{in}}} \mathcal{N}(z_j, \sigma_{z,j}) \delta(\alpha - \alpha_j) \delta(\beta - \beta_j), \quad (15)$$

where $\mathcal{N}(z_j, \sigma_{z,j})$ represents a Gaussian distribution centered at z_j , with a standard deviation $\sigma_{z,j}$ arising from the peculiar velocity of the j -th galaxy and we take $\sigma_z = (1+z) \frac{\sqrt{\langle v^2 \rangle}}{c} 78.79$. Under the assumption of $\sqrt{\langle v^2 \rangle} = 500 \text{ km s}^{-1}$, σ_z is around 0.0017 in the redshift range $[0, 0.05]$ ⁸⁰. Here we assign an equal weight to each galaxy in the localization volume for simplicity. A more rigorous way is to assign different weights to different galaxies, for example, replacing $1/N_{\text{in}}$ with ω_j that is the weight of the j -th galaxy, proportional to the stellar or star-forming luminosity⁸¹.

$p_0(z, \alpha, \beta)$ in Eq. (13) represents the prior distribution of galaxies in the Universe, which is set to be uniform in the comoving volume, and it is expressed as

$$p_0(z, \alpha, \beta) \propto \frac{d^2 V_C}{dz d\Omega} \propto \frac{d_C^2(z)}{H(z)}, \quad (16)$$

with V_C the comoving volume and d_C the comoving distance.

The normalization term $\gamma(H_0)$ in Eq. (13) can be written as

$$\gamma(H_0) = \int \mathcal{D}_{\text{det}}^{\text{GW}}(d_L(z, H_0), \alpha, \beta) \mathcal{D}_{\text{det}}^{\text{EM}}(z, \alpha, \beta) p_0(z, \alpha, \beta) dz d\alpha d\beta \quad (17)$$

where $\mathcal{D}_{\text{det}}^{\text{GW}}(d_L(z, H_0), \alpha, \beta)$ and $\mathcal{D}_{\text{det}}^{\text{EM}}(z, \alpha, \beta)$ represent the GW selection effect and the EM selection effect, respectively, reflecting that only the events exceeding the detection threshold can be taken into account⁶. The GW selection effect⁸² can be expressed as

$$\mathcal{D}_{\text{det}}^{\text{GW}}(d_L(z, H_0), \alpha, \beta) = \int_{d_{\text{GW}} > d_{\text{GW}}^{\text{th}}} p(\mathcal{D}_{\text{GW}}|d_L(z, H_0), \alpha, \beta) d\mathcal{D}_{\text{GW}}, \quad (18)$$

with

$$p(\mathcal{D}_{\text{GW}}|d_L(z, H_0), \alpha, \beta) = \begin{cases} 1, & \text{if } \rho > \rho_{\text{th}}, \\ 0, & \text{if } \rho < \rho_{\text{th}}, \end{cases} \quad (19)$$

where $\rho_{\text{th}} = 10$ is the threshold of SNR. Since the 2MASS galaxy catalog is complete in our considered redshift range ($z < 0.05$), all the potential host galaxies will be contained in this galaxy catalog. Thus, the EM selection effect⁶ can be expressed as

$$\mathcal{D}_{\text{det}}^{\text{EM}}(z) = \int_{\mathcal{D}_{\text{EM}} > \mathcal{D}_{\text{EM}}^{\text{th}}} p(\mathcal{D}_{\text{EM}}|z, \alpha, \beta) d\mathcal{D}_{\text{EM}} = \mathcal{H}(z_{\text{max}} - z), \quad (20)$$

where \mathcal{H} is the Heaviside step function and z_{max} is set to 0.05 in our analysis.

Using Eqs. (13)–(20), we can calculate the likelihood of a single GW event. The total likelihood of SMBHB events can be written as

$$p(\mathcal{D}_{\text{GW}}, \mathcal{D}_{\text{EM}}|H_0) = \prod_{k=1}^{N_{\text{SMBHB}}} p(\mathcal{D}_{\text{GW},k}, \mathcal{D}_{\text{EM},k}|H_0), \quad (21)$$

where N_{SMBHB} is the total number of SMBHB events and k represents the k -th GW event.

Extended Data Table 2 shows the constraint results from the mock GW dark-siren data with different q_{min} values. Unlike the bright-siren data giving almost identical results, the dark-siren data constrain H_0 tighter as q decreases. The reason is that when we simulate the dark-siren data, q affects not only SNRs of GWs but also the number of mock SMBHBs, and the effect of the number of mock SMBHBs is more dominated than the effect of SNRs for the dark-siren method.

Data Availability The data that support the results in this paper are available from the corresponding author upon reasonable request.

Code Availability The code `hasasia` is publicly available at <https://hasasia.readthedocs.io>, and the code to simulate the SMBHB catalog is publicly available at https://github.com/ChiaraMingarelli/nanohertz_GWs.

1. Abbott, B. P. *et al.* Observation of Gravitational Waves from a Binary Black Hole Merger. *Phys. Rev. Lett.* **116**, 061102 (2016). 1602.03837.
2. Schutz, B. F. Determining the Hubble Constant from Gravitational Wave Observations. *Nature* **323**, 310–311 (1986).
3. Dalal, N., Holz, D. E., Hughes, S. A. & Jain, B. Short grb and binary black hole standard sirens as a probe of dark energy. *Phys. Rev. D* **74**, 063006 (2006). astro-ph/0601275.
4. Palmese, A. *et al.* A statistical standard siren measurement of the Hubble constant from the LIGO/Virgo gravitational wave compact object merger GW190814 and Dark Energy Survey galaxies. *Astrophys. J. Lett.* **900**, L33 (2020). 2006.14961.
5. Del Pozzo, W. Inference of the cosmological parameters from gravitational waves: application to second generation interferometers. *Phys. Rev. D* **86**, 043011 (2012). 1108.1317.
6. Chen, H.-Y., Fishbach, M. & Holz, D. E. A two per cent Hubble constant measurement from standard sirens within five years. *Nature* **562**, 545–547 (2018). 1712.06531.
7. Abbott, B. P. *et al.* GW170817: Observation of Gravitational Waves from a Binary Neutron Star Inspiral. *Phys. Rev. Lett.* **119**, 161101 (2017). 1710.05832.

8. Abbott, R. *et al.* Constraints on the Cosmic Expansion History from GWTC–3. *Astrophys. J.* **949**, 76 (2023). 2111.03604.
9. Punturo, M. *et al.* The Einstein Telescope: A third-generation gravitational wave observatory. *Class. Quant. Grav.* **27**, 194002 (2010).
10. Abbott, B. P. *et al.* Exploring the Sensitivity of Next Generation Gravitational Wave Detectors. *Class. Quant. Grav.* **34**, 044001 (2017). 1607.08697.
11. Chen, H.-Y. Systematic Uncertainty of Standard Sirens from the Viewing Angle of Binary Neutron Star Inspirals. *Phys. Rev. Lett.* **125**, 201301 (2020). 2006.02779.
12. Amaro-Seoane, P. *et al.* Laser Interferometer Space Antenna (2017). 1702.00786.
13. Hu, W.-R. & Wu, Y.-L. The Taiji Program in Space for gravitational wave physics and the nature of gravity. *Natl. Sci. Rev.* **4**, 685–686 (2017).
14. Luo, J. *et al.* The first round result from the TianQin-1 satellite. *Class. Quant. Grav.* **37**, 185013 (2020). 2008.09534.
15. Okamoto, I. Electromagnetic extraction of energy from Kerr black holes. *Publ. Astron. Soc. Jap.* **58**, 1047 (2006). astro-ph/0506302.
16. Haiman, Z. Electromagnetic chirp of a compact binary black hole: A phase template for the gravitational wave inspiral. *Phys. Rev. D* **96**, 023004 (2017). 1705.06765.
17. Tamanini, N. Late time cosmology with LISA: probing the cosmic expansion with massive

- black hole binary mergers as standard sirens. *J. Phys. Conf. Ser.* **840**, 012029 (2017). 1612.02634.
18. Cai, R.-G., Tamanini, N. & Yang, T. Reconstructing the dark sector interaction with LISA. *JCAP* **05**, 031 (2017). 1703.07323.
19. Wang, L.-F., Zhao, Z.-W., Zhang, J.-F. & Zhang, X. A preliminary forecast for cosmological parameter estimation with gravitational-wave standard sirens from TianQin. *JCAP* **11**, 012 (2020). 1907.01838.
20. Zhao, Z.-W., Wang, L.-F., Zhang, J.-F. & Zhang, X. Prospects for improving cosmological parameter estimation with gravitational-wave standard sirens from Taiji. *Sci. Bull.* **65**, 1340–1348 (2020). 1912.11629.
21. Wang, L.-F., Jin, S.-J., Zhang, J.-F. & Zhang, X. Forecast for cosmological parameter estimation with gravitational-wave standard sirens from the LISA-Taiji network. *Sci. China Phys. Mech. Astron.* **65**, 210411 (2022). 2101.11882.
22. Wang, R. *et al.* Hubble parameter estimation via dark sirens with the LISA-Taiji network. *Natl. Sci. Rev.* **9**, nwab054 (2022). 2010.14732.
23. Zhu, L.-G. *et al.* Constraining the Hubble constant to a precision of about 1% using multi-band dark standard siren detections. *Sci. China Phys. Mech. Astron.* **65**, 259811 (2022). 2110.05224.
24. Hobbs, G. The Parkes Pulsar Timing Array. *Class. Quant. Grav.* **30**, 224007 (2013). 1307.2629.

25. Kramer, M. & Champion, D. J. The European Pulsar Timing Array and the Large European Array for Pulsars. *Class. Quant. Grav.* **30**, 224009 (2013).
26. McLaughlin, M. A. The North American Nanohertz Observatory for Gravitational Waves. *Class. Quant. Grav.* **30**, 224008 (2013). 1310.0758.
27. Hobbs, G. *et al.* The international pulsar timing array project: using pulsars as a gravitational wave detector. *Class. Quant. Grav.* **27**, 084013 (2010). 0911.5206.
28. Lentati, L. *et al.* European Pulsar Timing Array Limits On An Isotropic Stochastic Gravitational-Wave Background. *Mon. Not. Roy. Astron. Soc.* **453**, 2576–2598 (2015). 1504.03692.
29. Arzoumanian, Z. *et al.* The NANOGrav 12.5 yr Data Set: Search for an Isotropic Stochastic Gravitational-wave Background. *Astrophys. J. Lett.* **905**, L34 (2020). 2009.04496.
30. Abbott, R. *et al.* Upper limits on the isotropic gravitational-wave background from Advanced LIGO and Advanced Virgo’s third observing run. *Phys. Rev. D* **104**, 022004 (2021). 2101.12130.
31. Sesana, A., Vecchio, A. & Volonteri, M. Gravitational waves from resolvable massive black hole binary systems and observations with Pulsar Timing Arrays. *Mon. Not. Roy. Astron. Soc.* **394**, 2255 (2009). 0809.3412.
32. Lee, K. J. *et al.* Gravitational wave astronomy of single sources with a pulsar timing array. *Mon. Not. Roy. Astron. Soc.* **414**, 3251 (2011). 1103.0115.

33. Wang, Y. & Mohanty, S. D. Pulsar Timing Array Based Search for Supermassive Black Hole Binaries in the Square Kilometer Array Era. *Phys. Rev. Lett.* **118**, 151104 (2017). [Erratum: *Phys.Rev.Lett.* 124, 169901 (2020)], 1611.09440.
34. Nan, R. *et al.* The Five-Hundred-Meter Aperture Spherical Radio Telescope (FAST) Project. *Int. J. Mod. Phys. D* **20**, 989–1024 (2011). 1105.3794.
35. Lazio, T. J. W. The Square Kilometre Array pulsar timing array. *Class. Quant. Grav.* **30**, 224011 (2013).
36. Smits, R. *et al.* Pulsar searches and timing with the square kilometre array. *Astron. Astrophys.* **493**, 1161–1170 (2009). 0811.0211.
37. Yan, C., Zhao, W. & Lu, Y. On using inspiralling supermassive binary black holes in the PTA frequency band as standard sirens to constrain dark energy. *Astrophys. J.* **889**, 79 (2019). 1912.04103.
38. Valtonen, M. J. *et al.* A massive binary black-hole system in OJ 287 and a test of general relativity. *Nature* **452**, 851–853 (2008). 0809.1280.
39. Zhang, X. Gravitational wave standard sirens and cosmological parameter measurement. *Sci. China Phys. Mech. Astron.* **62**, 110431 (2019). 1905.11122.
40. Zhang, J.-F., Zhang, M., Jin, S.-J., Qi, J.-Z. & Zhang, X. Cosmological parameter estimation with future gravitational wave standard siren observation from the Einstein Telescope. *JCAP* **09**, 068 (2019). 1907.03238.

41. Jin, S.-J., He, D.-Z., Xu, Y., Zhang, J.-F. & Zhang, X. Forecast for cosmological parameter estimation with gravitational-wave standard siren observation from the Cosmic Explorer. *JCAP* **03**, 051 (2020). 2001.05393.
42. Bian, L. *et al.* The Gravitational-Wave Physics II: Progress. *Sci. China Phys. Mech. Astron.* **64**, 120401 (2021). 2106.10235.
43. Feng, Y., Li, D., Zheng, Z. & Tsai, C.-W. Supermassive Binary Black Hole Evolution can be traced by a small SKA Pulsar Timing Array. *Phys. Rev. D* **102**, 023014 (2020). 2005.11118.
44. Manchester, R. N., Hobbs, G. B., Teoh, A. & Hobbs, M. The Australia Telescope National Facility pulsar catalogue. *Astron. J.* **129**, 1993 (2005). astro-ph/0412641.
45. Porayko, N. K. *et al.* Parkes Pulsar Timing Array constraints on ultralight scalar-field dark matter. *Phys. Rev. D* **98**, 102002 (2018). 1810.03227.
46. Mingarelli, C. M. F. Probing supermassive black hole binaries with pulsar timing. *Nature Astronomy* **3**, 8–10 (2019). 1901.06785.
47. Hazboun, J., Romano, J. & Smith, T. Hasasia: A Python package for Pulsar Timing Array Sensitivity Curves. *J. Open Source Softw.* **4**, 1775 (2019).
48. Hazboun, J. S., Romano, J. D. & Smith, T. L. Realistic sensitivity curves for pulsar timing arrays. *Phys. Rev. D* **100**, 104028 (2019). 1907.04341.
49. Skrutskie, M. F. *et al.* The Two Micron All Sky Survey (2MASS). *Astron. J.* **131**, 1163–1183 (2006).

50. Jarrett, T. H. *et al.* 2mass extended source catalog: overview and algorithms. *Astron. J.* **119**, 2498–2531 (2000). astro-ph/0004318.
51. Graham, M. J. *et al.* A possible close supermassive black-hole binary in a quasar with optical periodicity. *Nature* **518**, 74 (2015). 1501.01375.
52. Graham, M. J. *et al.* A systematic search for close supermassive black hole binaries in the Catalina Real-Time Transient Survey. *Mon. Not. Roy. Astron. Soc.* **453**, 1562–1576 (2015). 1507.07603.
53. Charisi, M. *et al.* A Population of Short-Period Variable Quasars from PTF as Supermassive Black Hole Binary Candidates. *Mon. Not. Roy. Astron. Soc.* **463**, 2145–2171 (2016). 1604.01020.
54. Yan, C.-S., Lu, Y., Dai, X. & Yu, Q. A Probable Milli-parsec Supermassive Binary Black Hole in the Nearest Quasar mrk 231. *Astrophys. J.* **809**, 117 (2015). 1508.06292.
55. Li, Y.-R. *et al.* Spectroscopic Indication of a Centi-parsec Supermassive Black Hole Binary in the Galactic Center of Ngc 5548. *Astrophys. J.* **822**, 4 (2016). 1602.05005.
56. Zheng, Z.-Y. *et al.* SDSS J0159+0105: A Radio-Quiet Quasar with a Centi-Parsec Supermassive Black Hole Binary Candidate. *Astrophys. J.* **827**, 56 (2016). 1512.08730.
57. Li, Y.-R. *et al.* A Possible ~ 20 yr Periodicity in Long-term Optical Photometric and Spectral Variations of the Nearby Radio-quiet Active Galactic Nucleus Ark 120. *Astrophys. J. Suppl.* **241**, 33 (2019). 1705.07781.

58. Kelley, L. Z. *et al.* Multi-Messenger Astrophysics with Pulsar Timing Arrays (2019). 1903.07644.
59. Palenzuela, C., Lehner, L. & Liebling, S. L. Dual Jets from Binary Black Holes. *Science* **329**, 927 (2010). 1005.1067.
60. Hambleton, K. M. *et al.* Rubin Observatory LSST Transients and Variable Stars Roadmap (2022). 2208.04499.
61. Liske, J. *et al.* Cosmic dynamics in the era of Extremely Large Telescopes. *Mon. Not. Roy. Astron. Soc.* **386**, 1192–1218 (2008). 0802.1532.
62. Tamanini, N. *et al.* Science with the space-based interferometer eLISA. III: Probing the expansion of the Universe using gravitational wave standard sirens. *JCAP* **04**, 002 (2016). 1601.07112.
63. Aghanim, N. *et al.* Planck 2018 results. VI. Cosmological parameters. *Astron. Astrophys.* **641**, A6 (2020). [Erratum: *Astron. Astrophys.* 652, C4 (2021)], 1807.06209.
64. Zhan, H. The wide-field multiband imaging and slitless spectroscopy survey to be carried out by the survey space telescope of china manned space program. *Chin. Sci. Bull* **66**, 1290–1298 (2021).
65. Laureijs, R. *et al.* Euclid Definition Study Report (2011). 1110.3193.
66. Chen, Y., Yu, Q. & Lu, Y. Dynamical evolution of cosmic supermassive binary black holes and their gravitational wave radiation. *Astrophys. J.* **897**, 86 (2020). 2005.10818.

67. Mingarelli, C. M. F. *et al.* The Local Nanohertz Gravitational-Wave Landscape From Supermassive Black Hole Binaries. *Nature Astron.* **1**, 886–892 (2017). 1708.03491.
68. Ellis, J. A., Siemens, X. & Creighton, J. D. E. Optimal strategies for continuous gravitational wave detection in pulsar timing arrays. *Astrophys. J.* **756**, 175 (2012). 1204.4218.
69. Hirata, C. M., Holz, D. E. & Cutler, C. Reducing the weak lensing noise for the gravitational wave Hubble diagram using the non-Gaussianity of the magnification distribution. *Phys. Rev. D* **81**, 124046 (2010). 1004.3988.
70. Kocsis, B., Frei, Z., Haiman, Z. & Menou, K. Finding the electromagnetic counterparts of cosmological standard sirens. *Astrophys. J.* **637**, 27–37 (2006). astro-ph/0505394.
71. He, J.-h. Accurate method to determine the systematics due to the peculiar velocities of galaxies in measuring the Hubble constant from gravitational-wave standard sirens. *Phys. Rev. D* **100**, 023527 (2019). 1903.11254.
72. Jin, S.-J., Xing, S.-S., Shao, Y., Zhang, J.-F. & Zhang, X. Joint constraints on cosmological parameters using future multi-band gravitational wave standard siren observations. *Chin. Phys. C* **47**, 065104 (2023). 2301.06722.
73. McConnell, N. J. & Ma, C.-P. Revisiting the Scaling Relations of Black Hole Masses and Host Galaxy Properties. *Astrophys. J.* **764**, 184 (2013). 1211.2816.
74. Binney, J. & Tremaine, S. *Galactic Dynamics: Second Edition* (Princeton University Press, 2008).

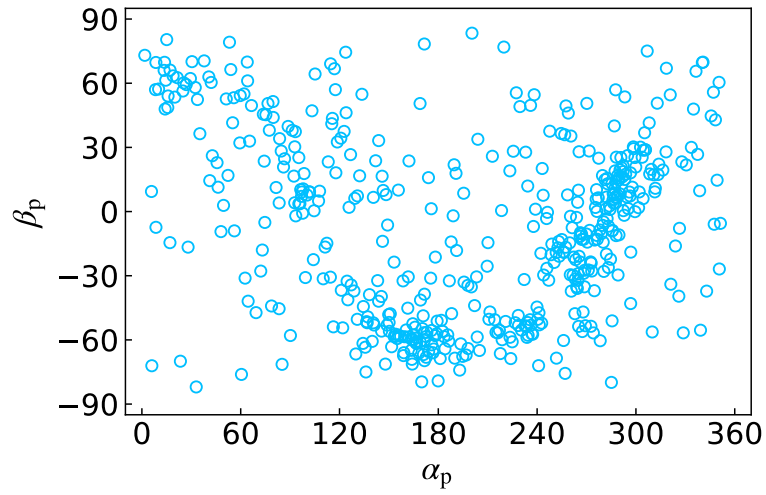
75. Sesana, A. & Khan, F. M. Scattering experiments meet N-body – I. A practical recipe for the evolution of massive black hole binaries in stellar environments. *Mon. Not. Roy. Astron. Soc.* **454**, L66–L70 (2015). 1505.02062.
76. Rodriguez-Gomez, V. *et al.* The merger rate of galaxies in the Illustris Simulation: a comparison with observations and semi-empirical models. *Mon. Not. Roy. Astron. Soc.* **449**, 49–64 (2015). 1502.01339.
77. Genel, S. *et al.* Introducing the Illustris Project: the evolution of galaxy populations across cosmic time. *Mon. Not. Roy. Astron. Soc.* **445**, 175–200 (2014). 1405.3749.
78. Hogg, D. W. Distance measures in cosmology (1999). astro-ph/9905116.
79. Muttoni, N., Laghi, D., Tamanini, N., Marsat, S. & Izquierdo-Villalba, D. Dark siren cosmology with binary black holes in the era of third-generation gravitational wave detectors (2023). 2303.10693.
80. Henriques, B. *et al.* Confronting theoretical models with the observed evolution of the galaxy population out to $z=4$. *Mon. Not. Roy. Astron. Soc.* **421**, 2904 (2012). 1109.3457.
81. Fishbach, M. *et al.* A standard siren measurement of the hubble constant from gw170817 without the electromagnetic counterpart. *The Astrophysical Journal Letters* **871**, L13 (2019).
82. Gray, R. *et al.* Cosmological inference using gravitational wave standard sirens: A mock data analysis. *Physical Review D* **101** (2020).

Correspondence Correspondence and requests for materials should be addressed to Xin Zhang (email: zhangxin@mail.neu.edu.cn).

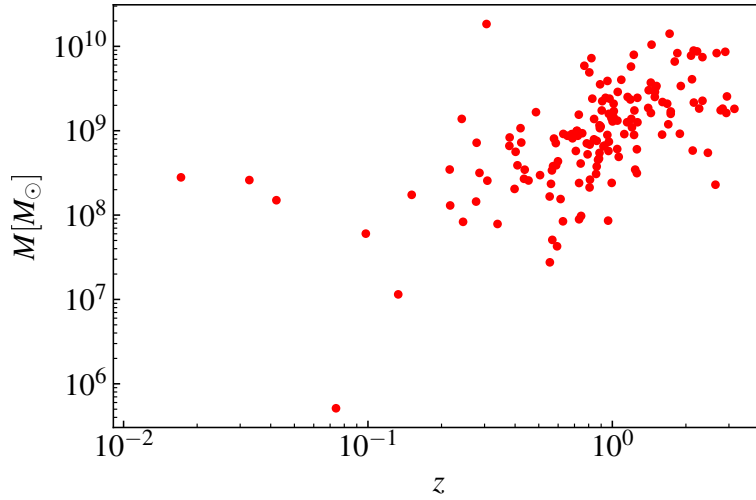
Acknowledgements We thank Guang-Peng Zhang for his contribution in the early stage of this work. We are grateful to Si-Ren Xiao, Shang-Jie Jin and Ji-Yu Song for fruitful discussions. This work was supported by the National SKA Program of China (Grants Nos. 2022SKA0110200 and 2022SKA0110203), the National Natural Science Foundation of China (Grants Nos. 11975072, 11835009, and 11875102), the science research grants from the China Manned Space Project (Grant No. CMS-CSST-2021-B01), the Liaoning Revitalization Talents Program (Grant No. XLYC1905011), the National Program for Support of Top-Notch Young Professionals (Grant No. W02070050), and the National 111 Project of China (Grant No. B16009).

Author contributions Ling-Feng Wang performed part of the computation, and wrote majority of the manuscript. Yue Shao performed majority of the computation, and wrote part of the manuscript. Jing-Fei Zhang wrote part of the manuscript. Xin Zhang proposed and led the study, and contributed to the collaboration organization and the manuscript writing. All authors discussed the results and commented on the manuscript.

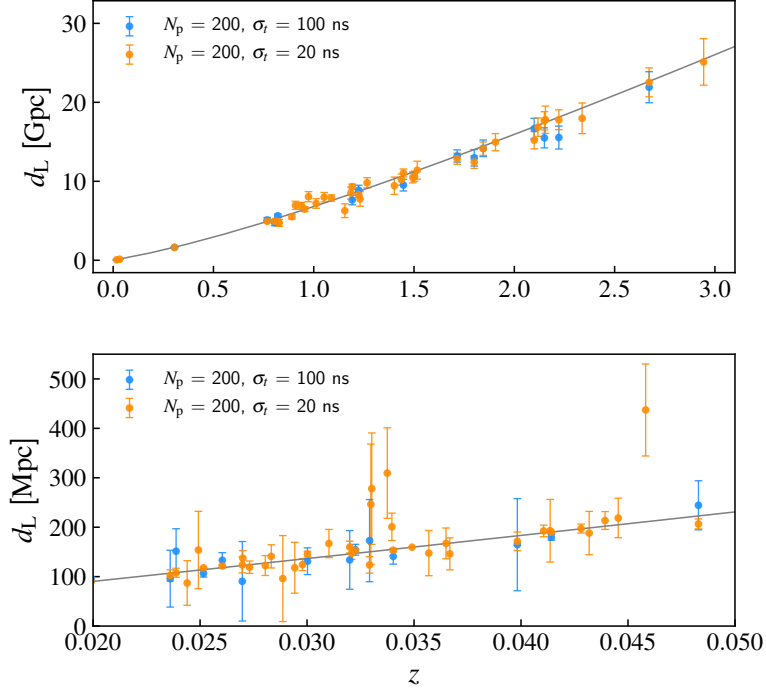
Competing Interests The authors declare no competing interests.



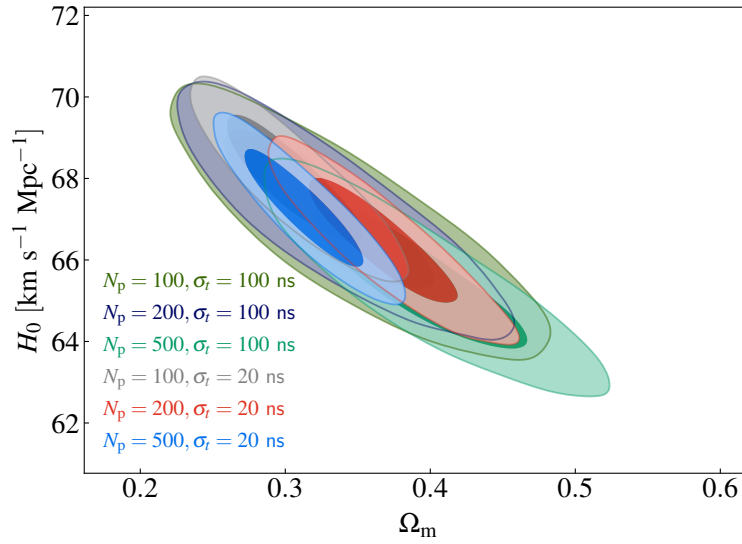
Extended Data Figure 1 | Positions of the selected MSPs on the sky. We select 500 pulsars within 3 kpc from the Earth obtained from the ATNF pulsar catalog⁴⁴.



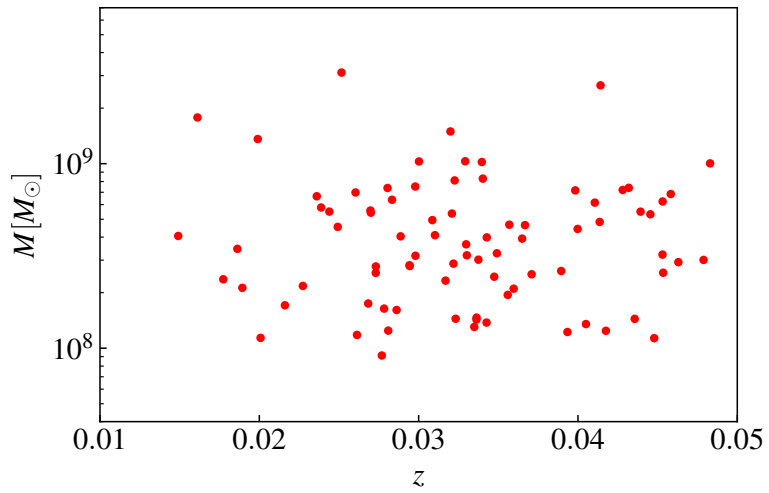
Extended Data Figure 2 | Distribution of 154 SMBHB candidates in the z - M plane, taken from Refs. ^{38,51-57}. These SMBHB candidates are used in the analysis of bright sirens.



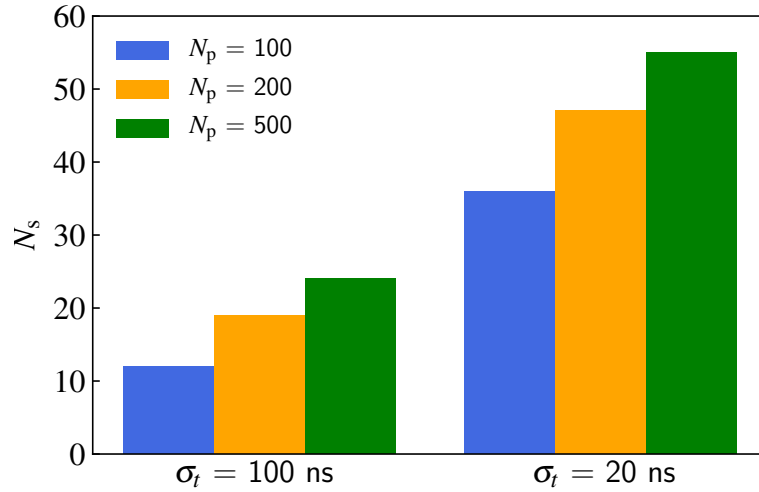
Extended Data Figure 3 | GW bright-siren and dark-siren data simulated from the 154 SMBHB candidates and 84 mock SMBHBs, respectively. Upper and lower panels correspond to the bright and dark sirens, respectively. The redshifts of dark sirens shown in lower panel are the redshifts of mock SMBHBs' host galaxies. The luminosity distances d_L are calculated based on the Λ CDM model in which the fiducial values of cosmological parameters are set to be the *Planck* 2018 results. The error bars of the data points (Δd_L) in the figure are obtained from the Fisher matrix. The central values of the data points are randomly chosen in the range of $[d_L - \Delta d_L, d_L + \Delta d_L]$. The data points with $\Delta d_L/d_L > 1$ are not displayed in the figure.



Extended Data Figure 4 | 2D marginalized contours (68.3% and 95.4% confidence level) in the Ω_m - H_0 plane for the Λ CDM model by using the PTA data. Here the PTA data refer to the mock GW bright-siren data.



Extended Data Figure 5 | Distribution of 84 SMBHBs simulated from the 2MASS catalog in the z - M plane. We use these SMBHBs in the analysis of dark sirens.



Extended Data Figure 6 | Numbers of SMBHBs with $N_{\text{in}} < 10$ in the analysis of dark sirens. N_s is the number of detected SMBHBs ($\rho > 10$). Here N_{in} is calculated by fixing $H_0 = 67.36 \text{ km s}^{-1} \text{ Mpc}^{-1}$. As N_p increases and σ_t decreases, more SMBHBs satisfy $N_{\text{in}} < 10$.

Data	N_p	$\sigma_t(\text{ns})$	$\sigma(\Omega_m)$	$\varepsilon(\Omega_m)$	$\sigma(H_0)$	$\varepsilon(H_0)$	$\sigma(w)$	$\varepsilon(w)$
CMB	–	–	0.054	0.179	6.0	0.858	0.20	0.185
PTA	100	100	0.083	0.407	3.9	0.056	0.50	0.424
	500	100	0.090	0.292	3.8	0.057	0.68	0.548
	100	20	0.053	0.157	3.6	0.053	0.63	0.460
CMB+PTA	100	100	0.014	0.042	1.4	0.020	0.053	0.055
	500	100	0.011	0.033	1.1	0.017	0.042	0.044
	100	20	0.010	0.031	1.1	0.017	0.045	0.047

Extended Data Table 1 | Relative errors of the cosmological parameters in the w CDM model using the CMB, PTA, and CMB+PTA data. N_s is the number of detected SMBHB ($\rho > 10$). Here the PTA data refer to the mock GW bright-siren data.

q_{\min}	bright siren			dark siren			
	N_s	$\sigma(H_0)$	$\varepsilon(H_0)$	N_{mock}	N_s	$\sigma(H_0)$	$\varepsilon(H_0)$
1	32	0.99	0.0147	54	34	1.41	0.0210
0.25	25	1.00	0.0147	84	41	1.25	0.0184
0.1	22	1.00	0.0147	134	65	1.21	0.0178
0.01	21	1.10	0.0165	197	87	1.15	0.0171

Extended Data Table 2 | Relative errors of H_0 in the Λ CDM model with different q_{\min} . N_{mock} and N_s are the numbers of mock SMBHBs and detected SMBHBs ($\rho > 10$), respectively, and $\varepsilon(H_0)$ is the relative error of H_0 . Here we set $N_p = 100$ and $\sigma_t = 20$ ns.